CrossMark

Synthesis, characterization, and morphological control of ZnMoO$_4$ nanostructures through precipitation method and its photocatalyst application

Majid Ramezani[1] · S. Mostafa Hosseinpour-Mashkani[2] · Ali Sobhani-Nasab[2] · Hadi Ghasemi Estarki[3]

Abstract Zinc molybdate rod-like nanostructures have been successfully synthesized by precipitation method process in the presence of different surfactants. This study aimed to investigate the effects of different surfactant such as sodium dodecyl sulfate, polyethylene glycol, and cetyltrimethylammonium bromide and solvent on the morphology and particle size of final products. It was found that the size and morphology of the products could be greatly influenced by the aforementioned parameters. To the best of authors' knowledge, this is the first report on the synthesis of ZnMoO$_4$ nanostructure with different morphologies in the presence of ethanol as a solvent. The as-synthesized products were characterized by XRD, SEM, UV–Vis, and EDS techniques. To evaluate the photocatalyst properties of nanocrystalline zinc molybdate, the photocatalytic degradation of methyl orange under visible light irradiation was carried out.

1 Introduction

In recent years, there has been considerable interest in nanocrystalline semiconductor particles, due to increase activity and a large surface-to-volume ratio and special optical and electrical properties as compared to those of the bulk materials [1–4]. Metal molybdates and tungstates have two types of structures, depending on the size of bivalentcations, scheelite (ionic radius >40.99 A: Ca, Sr, Ba, and Pb) and wolframite (ionic radius <0.77 A: Mg, Mn, Fe, Co, Ni, and Zn) [5–8]. They have attracted considerable interest for a number of researchers, due to their promising technological importance in a wide range of applications, including photoluminescence, scintillating materials, humidity sensors, photoelectric devices, photonic crystals, light weight filler materials, photocatalysts, and chemical reactors [9–14]. Several methods have been used to obtain ZnMoO$_4$ powders, such as czochralski and kyropoulos method, hydrothermal synthesis, full-potential linear-augmented-plane-wave method [15–19]. Zinc cations have been reported to be very interesting as 'inorganic nodes' in the design of porous inorganic compounds or metal organic framework compounds. Hence, studies on zinc molybdenum compounds are not only for catalytic purposes but also to investigate substances with complex architecture. It is very interesting that zinc molybdate includes monoclinic (ZnMoO$_4$) and triclinic (α-ZnMoO$_4$) structures, and the structure of ZnMoO$_4$ is more complex than that of MMoO$_4$ (M = Mn, Co) [20–23]. Here, we report the synthesis and characterization of ZnMoO$_4$ through the precipitation method. Besides, several experiments were performed in order to investigate the effect of surfactants such as sodium dodecyl sulfate (SDS), polyethylene glycol (PEG), and cetyltrimethylammonium bromide (CTAB) and solvent on the morphology and particle size of final products. The photocatalytic degradation was investigated using methyl orange (MO) under visible light irradiation ($\lambda > 400$ nm). The resulting degradation rates of the methyl orange were measured to be as high as 90 % in 6 h.

✉ Ali Sobhani-Nasab
ali.sobhaninasab@gmail.com

[1] Department of Chemistry, Arak Branch, Islamic Azad University, Arak, Iran

[2] Young Researchers and Elites Club, Arak Branch, Islamic Azad University, Arak, Iran

[3] Department of Analytical Chemistry, Faculty of Chemistry, University of Kashan, 87317-51167 Kashan, Iran

2 Experimental

2.1 Characterization

X-ray diffraction (XRD) patterns were recorded by a Philips-X'PertPro, X-ray diffractometer using Ni-filtered Cu Kα radiation at scan range of $10 < 2\theta < 80$. Scanning electron microscopy (SEM) images were obtained on LEO-1455VP equipped with an energy dispersive X-ray spectroscopy. The energy dispersive spectrometry (EDS) analysis was studied by XL30, Philips microscope. UV–Vis diffuse reflectance spectroscopy analysis (UV–Vis) was carried out using shimadzu UV–Vis scanning spectrometer.
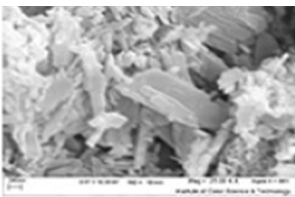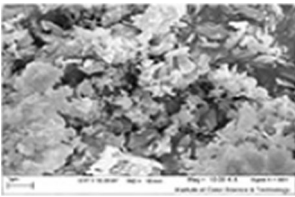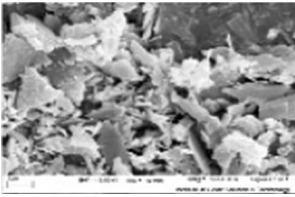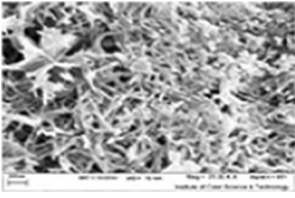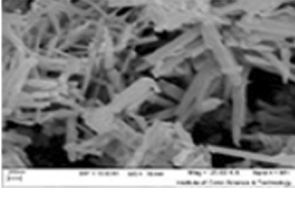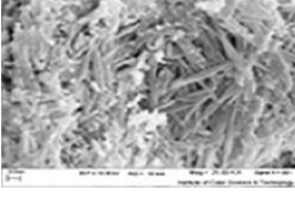
2.2 Synthesis of ZnMoO$_4$ nanostructures

The zinc nitrate ($Zn(NO_3)_2 \cdot 6H_2O$, $(NH_4)_6Mo_7O_{24} \cdot 4H_2O$ were purchased from Merck Company and used without further purification. In a typical synthesis, the stoichiometric amount of $(NH_4)_6Mo_7O_{24} \cdot 4H_2O$ (1 mmol), was dissolved in 20 ml distilled water under stirring to form a homogeneous solution. Afterwards, 7 mmol of $Zn(NO_3)_2 \cdot 6H_2O$ and SDS as surfactant were dissolved in distilled water and added to the above solution under constant stirring. Subsequently, the system was allowed to cool to room temperature naturally, the obtained precipitate was collected by filtration, then washed with absolute ethanol, and distilled water several times. Finally, the product was dried in vacuum at 90 °C for 2 h. Reaction conditions are listed in Table 1. Schematic diagram of formation of ZnMoO$_4$ nanostructures is depicted in Scheme 1.

2.3 Photocatalytic experimental

The methyl orange (MO) photodegradation was examined as a model reaction to evaluate the photocatalytic activities of the ZnMoO$_4$ nanostructures. The photocatalytic experiments were performed under an irradiation wavelength of $\lambda > 400$ nm. The photocatalytic activity of nanocrystalline zinc molybdate obtained from sample no. 5 was studied by the degradation of methyl orange solution as a target pollutant. The photocatalytic degradation was performed with 150 mL solution of methyl orange (0.0005 g) containing 0.05 g of ZnMoO$_4$. This mixture was aerated for 30 min to reach adsorption equilibrium. Later, the mixture was placed inside the photoreactor in which the vessel was 15 cm away from the visible source of 400 W Xeno lamp. The photocatalytic test was performed at room temperature. Aliquots of the mixture were taken at definite interval of times during the irradiation, and after centrifugation they were analyzed by a UV–Vis spectrometer. The methyl orange (MO) degradation percentage was calculated as:

Table 1 Reaction conditions for ZnMoO$_4$ nanostructures

Sample no	Solvent	Surfactant	SEM
1	Water	SDS	
2	Water	PEG	
3	Water	CTAB	
4	Ethanol	SDS	
5	Ethanol	PEG	
6	Ethanol	CTAB	

$$\text{Degradation rate} (\%) = \frac{A_0 - A}{A_0} \times 100$$

where A_0 and A are the absorbance value of solution at A_0 and A min, respectively.

3 Results and discussion

Figure 1 shows a typical XRD pattern ($10° < 2\theta < 80°$) of ZnMoO$_4$ nanostructures (sample 5). Based on the Fig. 1, the patterns agree well with the reported patterns for zinc

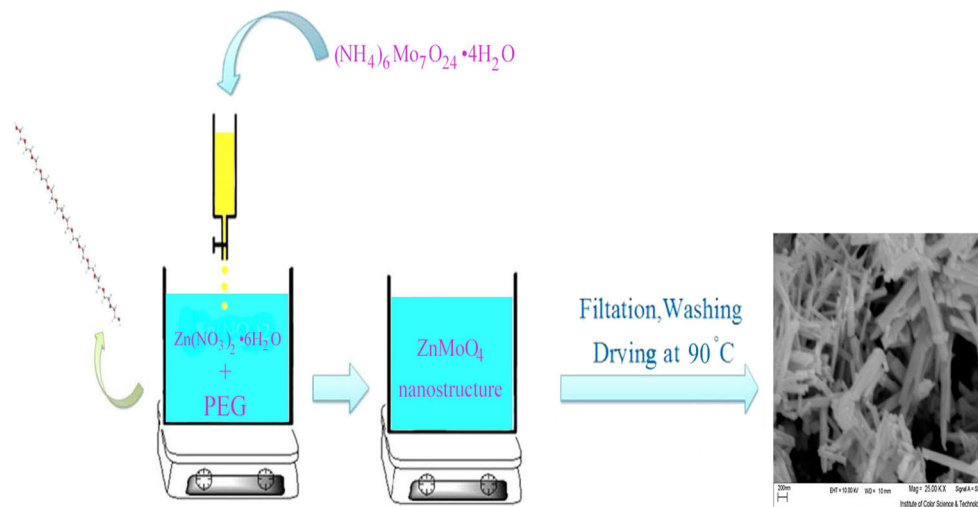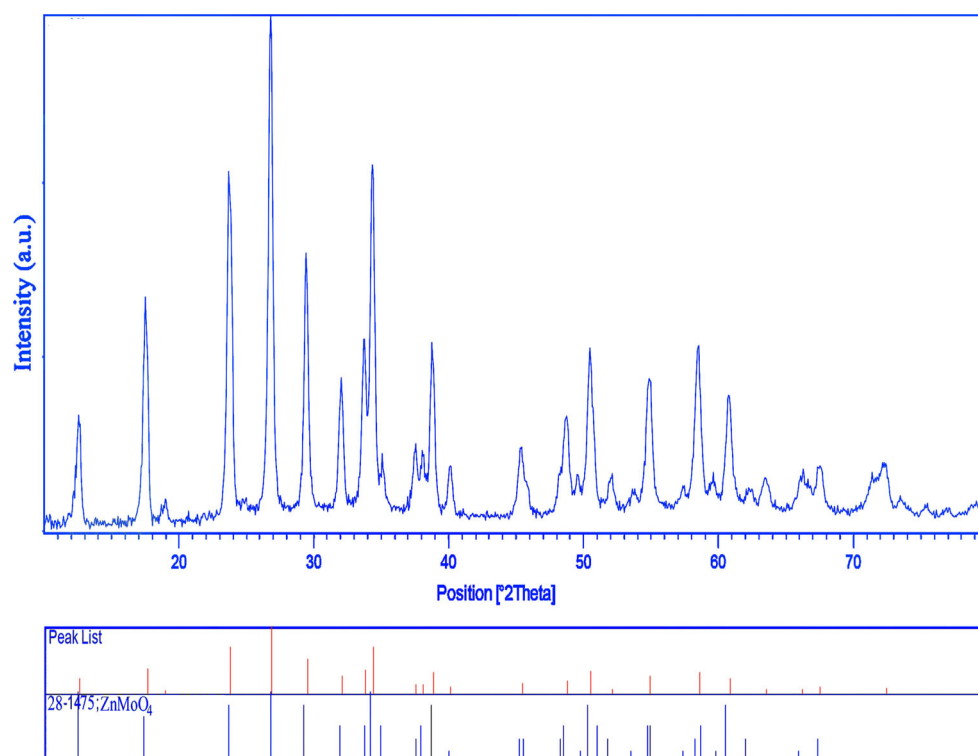**Scheme 1** Schematic diagram illustrating the formation of $ZnMoO_4$ nanostructures

Fig. 1 XRD pattern of $ZnMoO_4$ nanostructures (sample no. 5)

molybdate (JCPDS No: 28-1475). From XRD data, the crystallite diameter (D_c) of $ZnMoO_4$ nanostructures obtained from sample 5 was calculated to be 35 nm using the Scherer equation [24]:

$$D_c = K\lambda / \beta \cos \theta$$

where β is the breadth of the observed diffraction line at its half intensity maximum, K is the so-called shape factor, which usually takes a value of about 0.9, and λ is the wavelength of X-ray source used in XRD. It is well-known that the presence of surfactant during the production of

nano-sized materials has a great effect on the shape and particle size of products. Therefore, much attention has been paid to the study of such supramolecular structures, which can play an important role as both template and microreactore for producing nanomaterials. For example, sodium dodecyl sulfate (SDS) molecules as an anionic surfactant can self-aggregate into cubic, hexagonal and lamellar structures [25, 26].

In recent years, there has been considerable interest in control the shape and particle size of nanostructures through the control reaction parameters thanks to the fact
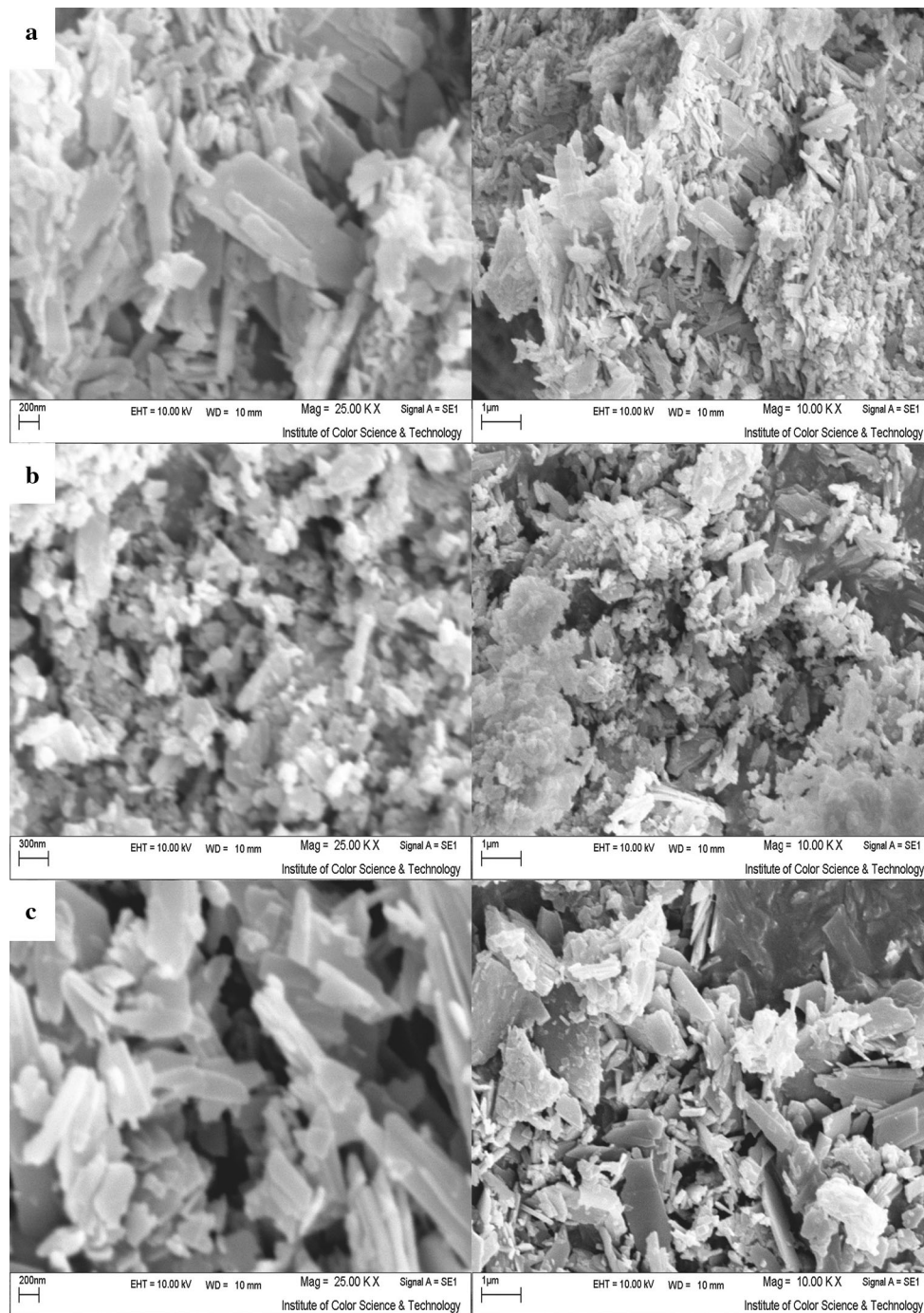
Fig. 2 SEM images of ZnMoO$_4$ nanostructures. **a** Sample no. 1, **b** sample no. 2, **c** sample no. 3

that properties of nanostructures are highly depend on their particle size and shape; therefore, we performed several experiments to investigate the effect of surfactants such as SDS, PEG, and CTAB and solvent on the morphology and particle size of the ZnMoO$_4$ nanostructures. Figure 2a–c shows the SEM images of ZnMoO$_4$ in the presence of water as a solvent and SDS, PEG, and CTAB as surfactants accordance with sample 1–3, respectively. According to

the Fig. 2a–c, the products mainly consist of nanosheets; however, use SDS as surfactant causes decrease in the size of nanosheets structure. To investigate the effect of water as a solvent three experiments were performed with ethanol in the presence of same surfactants SDS, PEG, and CTAB accordance with sample 4–6 (Fig. 3a–c), respectively. Based on the Fig. 3a–c, in the presence of ethanol with same surfactant the morphology of products were changed
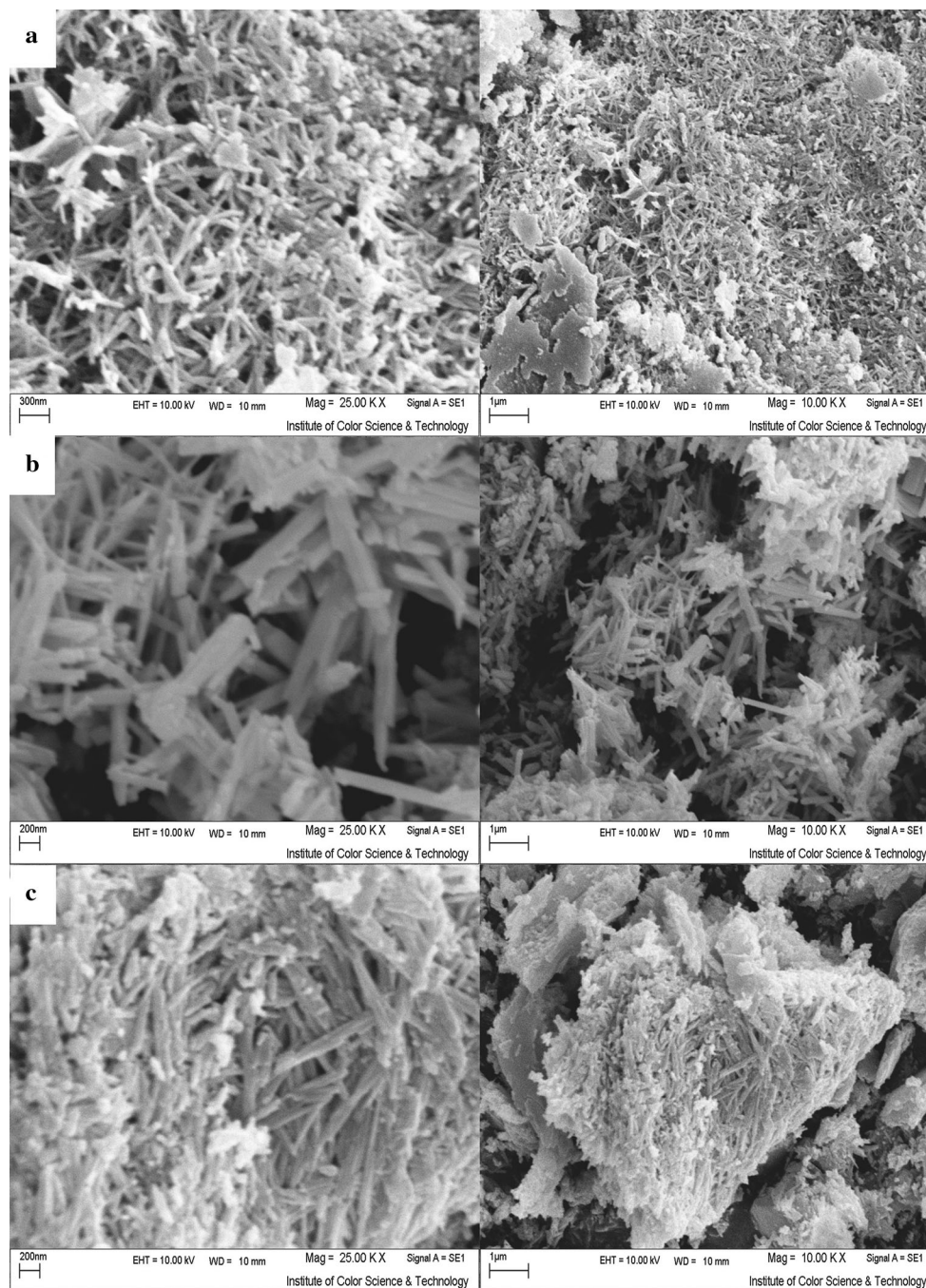
Fig. 3 SEM images of ZnMoO$_4$ nanostructures. **a** Sample no. 4, **b** sample no. 5, **c** sample no. 6

from nanosheets to nano rod structure. Furthermore, ethanol as a solvent causes decrease in particle size of final products. Chemical composition and purity of the as-synthesized ZnMoO$_4$ nanostructures was investigated by EDS analysis. The EDS spectrum of ZnMoO$_4$ obtained from sample 5 is shown in Fig. 4. According to the Fig. 4, Zn, O, and Mo elements are observed in the EDS spectrum. In addition, neither N nor C signals were detected in the EDS spectrum, which means the product is pure and free of any

surfactant or impurity. The diffused reflectance spectrum of the as-prepared ZnMoO$_4$ nanostructures (sample 5) is shown in Fig. 5. Using Tauc's formula, the band gap can be obtained from the absorption data. The energy gap (Eg) of the nanocrystalline ZnMoO$_4$ has been estimated by extrapolating the linear portion of the plot of $(\alpha h\nu)^2$ against $h\nu$ to the energy axis. The Eg value of the nanocrystalline ZnMoO$_4$ was calculated to be 2.76 eV. Photodegradation of methyl orange under UV light irradiation (Fig. 6a–c)
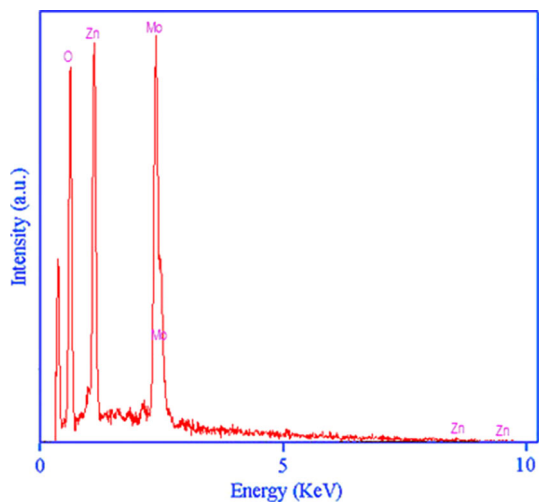
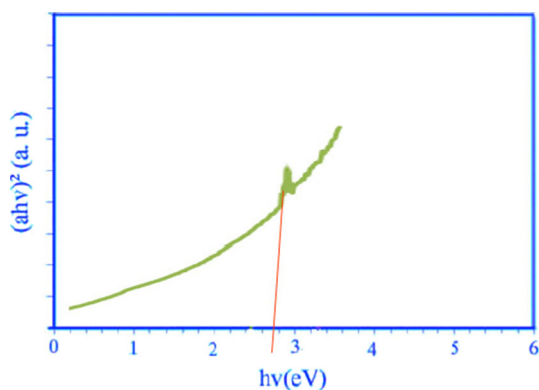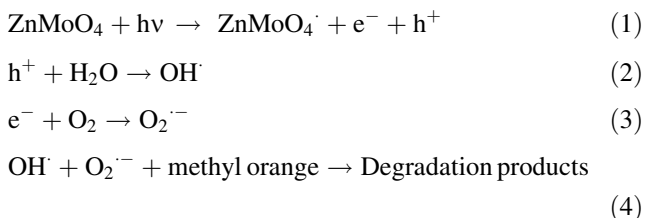**Fig. 4** EDS pattern of ZnMoO$_4$ nanostructures (sample no. 5)

Fig. 5 UV–Vis pattern of ZnMoO$_4$ nanostructures (sample no. 5)

Fig. 6 a Photocatalytic methyl orange degradation of ZnMoO$_4$ nanostructures (sample no. 5) under visible light, **b** fluorescence spectral time scan of methyl orange illuminated at 365 nm with ZnMoO$_4$ nanostructures and **c** reaction mechanism of methyl orange photodegradation over ZnMoO$_4$ under visible light irradiation

was employed to evaluate the photocatalytic activity of the as-synthesized ZnMoO$_4$ (sample no. 5). No methyl orange was practically broken down after 6 h without using visible light irradiation or nanocrystalline ZnMoO$_4$. This observation indicated that the contribution of self-degradation was insignificant. The probable mechanism of the photocatalytic degradation of methyl orange can be summarized as follows:

$$ZnMoO_4 + h\nu \rightarrow ZnMoO_4^{\cdot} + e^- + h^+ \tag{1}$$

$$h^+ + H_2O \rightarrow OH^{\cdot} \tag{2}$$

$$e^- + O_2 \rightarrow O_2^{\cdot -} \tag{3}$$

$$OH^{\cdot} + O_2^{\cdot -} + methyl\,orange \rightarrow Degradation\,products \tag{4}$$

Using photocatalytic calculations by Eq. (1), the methyl orange degradation was about 90 % after 6 h under irradiation of visible light and nanocrystalline ZnMoO$_4$ presented high photocatalytic activity (Fig. 6a). The spectrofluorimetric time-scans of methyl orange solution
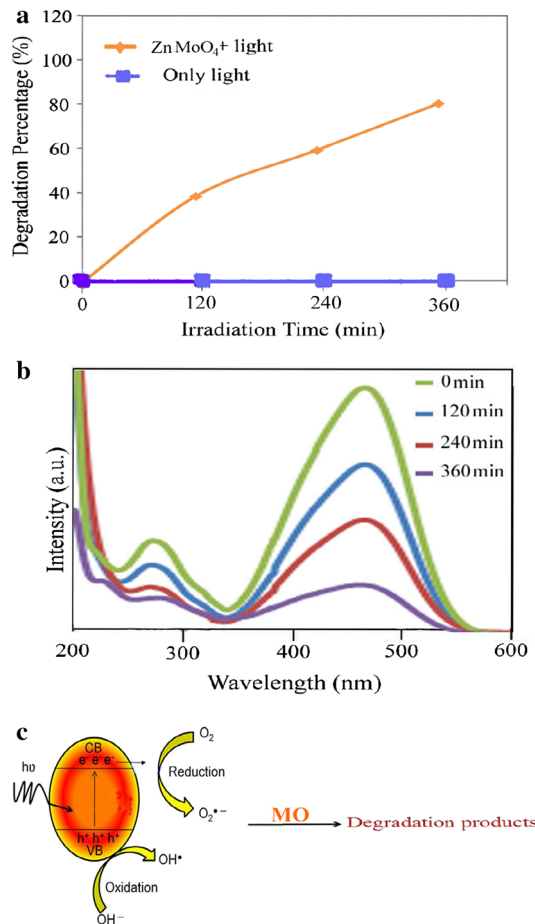
illuminated at 365 nm with nanocrystalline ZnMoO$_4$ are depicted in Fig. 6b. Figure 6b shows the continuous removal of methyl orange on the ZnMoO$_4$ under visible light irradiation. It is generally accepted that the heterogeneous photocatalytic processes comprise various steps (diffusion, adsorption, reaction, and etc.), and suitable distribution of the pore in the catalyst surface is effective and useful to diffusion of reactants and products, which prefer the photocatalytic reaction. In this investigation, the enhanced photocatalytic activity can be related to appropriate distribution of the pore in the nanocrystalline ZnMoO$_4$ surface, high hydroxyl amount and high separation rate of charge carriers (Fig. 6c) [27].

4 Conclusions

In this work, ZnMoO$_4$ nanostructures were successfully synthesized by a precipitation method. Besides, the effect of preparation parameters such as type surfactants and

solvent on the morphology, particle size, and crystal structure of $ZnMoO_4$ nanostructures were studied by SEM. Sodium dodecyl sulfate (SDS), polyethylene glycol (PEG), and cetyltrimethylammonium bromide (CTAB) were used as the surfactant. SEM results indicate that type of solvent as well as surfactants play an important role in the morphology and particle size of $ZnMoO_4$ nanostructures. When as-prepared nanocrystalline $ZnMoO_4$ was utilized as photocatalyst, the percentage of methyl orange degradation was about 90 % after 6 h irradiation under visible light.

Conflict of interest The author declares that the research was conducted in the absence of any commercial or financial relationships that could be construed as a potential conflict of interest.

References

1. M. Ramezani, A. Davoodi, A. Malekizad, S.M. Hosseinpour-Mashkani, J. Mater. Sci. Mater. Electron. **26**, 3957 (2015)
2. A. Javidan, S. Rafizadeh, S.M. Hosseinpour-Mashkani, Mater. Sci. Semicond. Process. **27**, 468 (2014)
3. S.M. Hosseinpour-Mashkani, M. Ramezani, Mater. Lett. **130**, 259 (2014)
4. F. Davara, M. Salavati-Niasari, J. Alloys Compd. **509**, 2487 (2011)
5. W.S. Wang, L. Zhen, C.Y. Xu, W.Z. Shao, Z.L. Chen, J. Alloys Compd. **529**, 17 (2012)
6. D. Li, Y.F. Zhu, Cryst. Eng. Commun. **14**, 1128 (2012)
7. H.W. Liu, L. Tan, Ionics **16**, 57 (2010)
8. L. Zhen, W.S. Wang, C.Y. Xu, W.Z. Shao, M.M. Ye, Z.L. Chen, Scripta Mater. **58**, 461 (2008)
9. L. Zhou, W. Wang, H. Xu, S. Sun, Cryst. Growth Des. **8**, 3595 (2008)
10. W.S. Wang, L. Zhen, C.Y. Xu, W.Z. Shao, Cryst. Growth Des. **9**, 1558 (2009)
11. A. Phuruangrat, N. Ekthammathat, T. Thongtem, S. Thongtem, J. Phys. Chem. Solids **72**, 176 (2011)
12. D. Zhu, K. Ki, X. Chen, T. Ying, J. Optoelectron. Adv. Mater. **5**, 403 (2011)
13. Q.L. Dai, G.G. Zhang, P. Liu, J. Wang, J.K. Tang, Inorg. Chem. **51**, 9232 (2012)
14. X. Jiang, J. Ma, B. Lin, Y. Ren, J. Liu, X. Zhu, J. Tao, J. Am. Ceram. Soc. **90**, 977 (2007)
15. G. Zhanga, S. Yua, Y. Yanga, W. Jianga, S. Zhanga, B. Huang, J. Cryst. Growth **312**, 1866 (2007)
16. L. Gironi, C. Arnaboldia, J.W. Beeman, O. Cremonesi, F.A. Danevich, V.Y. Degoda, L.I. Ivleva, L.L. Nagornaya, M. Pavan, G. Pessina, S. Pirro, V.I. Tretyak, I.A. Tupitsyna, J. Instrum. **5**, 11007 (2010)
17. L. Lv, W. Tong, Y. Zhang, Y. Su, X. Wang, J. Nanosci. Nanotechnol. **11**(11), 9506 (2011)
18. D.A. Spassky, A.N. Vasil'ev, I.A. Kamenskikh, V.V. Mikhailin, A.E. Savon, Y.A. Hizhnyi, S.G. Nedilko, P.A. Lykov, J. Phys. Condens. Matter **23**(36), 365501 (2011)
19. L.I. Ivleva, I.S. Voronina, L.Y. Berezovskaya, P.A. Lykov, V.V. Osiko, L.D. Iskhakova, Crystallogr. Rep. **53**, 1087 (2008)
20. G. Zhang, S. Yu, Y. Yang, W. Jiang, S. Zhang, B. Huang, J. Cryst. Growth **312**, 1866 (2010)
21. S.C. Abrahams, J. Chem. Phys. **46**, 2052 (1967)
22. M. Grzywa, W. Lasocha, W. Surga, J. Solid State Chem. **180**, 1590 (2007)
23. S.M. Hosseinpour-Mashkani, M. Ramezani, M. Vatanparast, Mater. Sci. Semicond. Process. **26**, 112 (2014)
24. Z. Shahri, M. Bazarganipour, M. Salavati-Niasari, Superlattices Microstruct. **63**, 258 (2013)
25. K. Vinodgopal, Y. He, M. Ashokkumar, F. Grieser, J. Phys. Chem. B **110**, 3849 (2006)
26. Y. Xie, X. Zheng, X. Jiang, J. Lu, L. Zhu, Inorg. Chem. **41**, 387 (2002)
27. J. Zhong, J. Li, F. Feng, Y. Lu, J. Zeng, W. Hu, Z. Tang, J. Mol. Catal. A Chem. **357**, 101 (2012)